Eur. Phys. J. Spec. Top.
https://doi.org/10.1140/epjs/s11734-026-02557-8

THE EUROPEAN PHYSICAL JOURNAL SPECIAL TOPICS

Regular Article

Reconstruction of EEG signals using next-generation reservoir computing

Artem Badarin[1,2,a], Fedor Ratnikov[3,b], and Andrey Andreev[1,2,c]

[1] Research Institute of Applied Artificial Intelligence and Digital Solutions, Plekhanov Russian University of Economics, 36, Stremyanny Per., 115054 Moscow, Russia
[2] Saratov State University, 83, Astrakhanskaya Str., 410012 Saratov, Russia
[3] HSE University, 11, Pokrovsky Bulvar, 109028 Moscow, Russia

Received 30 May 2026 / Accepted 26 July 2026

Abstract EEG recordings are often affected by the loss or corruption of individual channels due to electrode detachment, poor scalp contact, or external interference. Such channels must be accurately reconstructed before further analysis. In this study, we investigate Next-Generation Reservoir Computing (NG-RC) as a data-driven approach for reconstructing corrupted EEG channels and compare its performance with spherical spline interpolation implemented in MNE-Python. Using an 18-channel dataset from 24 healthy participants, we reconstruct each channel from the remaining channels and assess reconstruction quality in six frequency ranges: δ (1–4 Hz), θ (4–8 Hz), α (8–13 Hz), β (13–30 Hz), γ (30–40 Hz), and the full 1–40 Hz range. On noise-free data, NG-RC outperforms spline interpolation across all channels and frequency bands, with the most pronounced improvements observed in the high-frequency β and γ ranges and over frontal and central regions. Under additive Gaussian noise of increasing intensity, the performance of both methods decreases monotonically; however, NG-RC consistently remains more accurate, and the performance gap between the methods widens as noise intensity increases. This advantage is especially evident in the β and γ bands, where spline interpolation deteriorates substantially. These findings suggest that NG-RC provides a robust data-driven alternative for recovering corrupted or missing EEG channels in noise-prone recordings.

1 Introduction

Electroencephalography (EEG) is a widely used non-invasive neuroimaging modality with high temporal resolution [1, 2], essential for diagnosing and managing epilepsy [3, 4], sleep disorders [5, 6], stroke [7], encephalopathies [8], and traumatic brain injury [9]. It is used in clinical diagnostics, including epilepsy monitoring [10] and sleep staging, to cognitive neuroscience [11] and brain–computer interfaces (BCIs) [12–14]. However, EEG data are susceptible to various artifacts, originating from physiological sources (such as ocular, muscular, and cardiac activity) as well as environmental and instrumental interference [15]. Beyond transient artifacts, technical issues like electrode detachment, drying conductive gel, or wire failure can lead to persistently corrupted or entirely missing channels. Such data loss disrupts the spatial integrity of the recordings and severely complicates subsequent analyses, from source localization to multivariate pattern classification.

The standard method for recovering bad or missing EEG channels is interpolation. Spherical spline interpolation, popularized by its implementation in the MNE-Python software suite [16], is the most widely used method [17]. This technique estimates the potential at a faulty electrode by linearly combining signals from nearby channels based on a physically plausible model of scalp potential distribution. While computationally efficient and clinically validated, the method has a fundamental limitation: its interpolation weights follow from a fixed spatial model rather than being learned from the data, so it relies only on instantaneous spatial correlations and exploits neither the temporal structure of the recording nor any nonlinear structure in the relationship between channels. Whether

[a] e-mail: badarin.a.a@mail.ru (corresponding author)
[b] e-mail: fratnikov@hse.ru
[c] e-mail: andreevandrei1993@gmail.com

these sources of information improve reconstruction is an empirical question, which a data-driven approach is well suited to address.

In a parallel domain, machine learning has increasingly offered powerful tools for time-series modeling. Reservoir computing (RC), in particular, provides a framework for processing dynamical systems [18–23]. Classical RC employs a fixed, randomly initialized recurrent neural network, a "reservoir", to nonlinearly map input sequences into a high-dimensional space, where the desired output can be recovered by training only a simple linear readout layer [24]. A more recent variant, Next-Generation Reservoir Computing (NG-RC), was introduced by Gauthier et al. [25]. NG-RC replaces the opaque, random reservoir with a transparent, deterministic feature vector composed of time-delayed inputs and their polynomial combinations. This approach eliminates randomness, reduces the number of hyperparameters, and has shown state-of-the-art results in forecasting chaotic dynamics [25, 26] and reconstructing spatiotemporal systems from limited observations [27]. Its explicit feature space makes the model's behavior easy to interpret.

Despite its promise, the application of NG-RC to EEG signal processing remains largely unexplored. EEG is a challenging signal for this task: it is highly non-stationary, characterized by distinct oscillatory rhythms spanning a wide frequency spectrum (from slow delta waves to fast gamma oscillations), and exhibits intricate inter-channel dependencies. A systematic investigation of a transparent, next-generation reservoir computer for this task, and particularly its behavior in the presence of noise, has not yet been systematically studied.

In this article, we present a comprehensive investigation of NG-RC for the reconstruction of EEG signals, including channels degraded by additive noise. We propose a tailored NG-RC pipeline for multichannel EEG recovery, featuring a leave-one-out epoch-based hyperparameter optimization strategy. We evaluate reconstruction performance across canonical EEG frequency bands (delta, theta, alpha, beta, gamma, and full-spectrum), providing a detailed profile of the method's spectral fidelity in direct comparison with the standard spherical spline interpolation from MNE-Python. We assess the noise robustness of both NG-RC and spline interpolation by systematically contaminating all channels with additive noise of varying amplitudes and measuring the resultant degradation in reconstruction accuracy.

Our findings indicate that the NG-RC model consistently outperforms the conventional approach, especially in higher frequency regimes where the temporal structure of the signals is most informative, and remains robust to measurement noise. These results establish NG-RC as a compelling data-driven alternative for EEG signal recovery, with potential for applications in artifact correction.

The remainder of this paper is organized as follows. Section 2 describes the experimental EEG dataset, the NG-RC architecture and its training protocol, the MNE-Python spline interpolation baseline, and the performance metrics used for evaluation. Section 3 presents the findings, including the frequency-band-resolved reconstruction quality on clean signals and the noise robustness analysis. Finally, Sect. 4 summarizes the main contributions, discusses the limitations of the study, and outlines directions for future investigation.

2 Methods

2.1 Experimental EEG data

As experimental data we use 18 EEG signals recorded using a NeoRec cap 21 system according to the international 10–20 system: Fp1, Fp2, F3, F4, C3, C4, P3, P4, O1, O2, F7, F8, T7, T8, P7, P8, Cz, and Pz. The reference electrodes and ground electrodes were placed at Fz and Fpz, respectively. EEG signals were recorded at a sampling rate of 500 Hz and then bandpass filtered in the range of 1–40 Hz to remove low-frequency drift and high-frequency noise.

The detailed description of the experiment can be found in [28]. Twenty-four healthy volunteers (aged 20–32 years; mean age 25.3 ± 3.4 years) participated in the study. Data for each participant consists of the 60 epochs of 5 s duration corresponding to the perception of abstract and realistic stimuli for the left and right hands.

2.2 Next-generation reservoir computing

To recover the signals, we utilize a Next-Generation Reservoir Computing (NG-RC) architecture introduced in [25]. NG-RC represents a fully data-driven alternative to conventional reservoir computing, particularly suited for temporal data processing tasks including signal reconstruction and prediction. The core principle involves building an extended feature representation from time-lagged input variables and their nonlinear transformations (see Fig. 1).

We now describe the construction of the augmented feature vector. At a given time step i, the system receives N_{in} input channels, represented as $\mathbf{X}_i = [X_{i1}, X_{i2}, \ldots, X_{iN_{\mathrm{in}}}]^{\mathrm{T}}$. To incorporate temporal dependencies, we employ

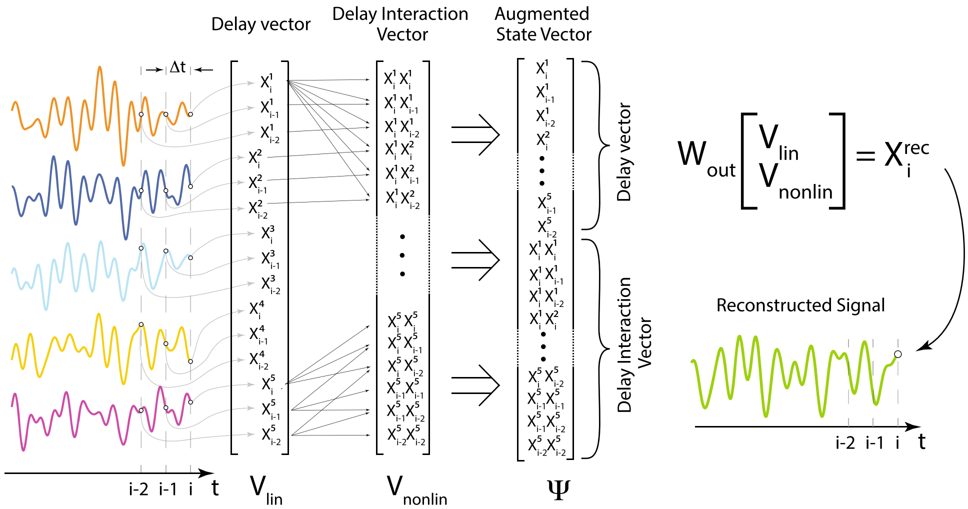

Fig. 1 Schematic representation of the extended state vector formation, including $k = 2$ delays for each input signal, taken at intervals of Δt (linear part), along with their pairwise products (nonlinear part, $p = 2$). W_{out} represents the trained matrix of output weights, and $X_{\text{rec},\,i}$ is the reconstructed signal at time step i

k delayed versions of the input, with a fixed lag of Δt between consecutive delays. The linear portion of the feature vector is assembled by concatenating these time-shifted signals:

$$\mathbf{V}_{\text{lin}} = \mathbf{X}_i \;\oplus\; \mathbf{X}_{i-\Delta t} \;\oplus\; \mathbf{X}_{i-2\Delta t} \;\oplus\; \cdots \;\oplus\; \mathbf{X}_{i-k\Delta t}, \tag{1}$$

where k denotes the total number of historical snapshots, and Δt is the spacing between them.

The nonlinear extension of the feature space is obtained by applying a polynomial expansion to the linear features. Following the formulation in [25], the nonlinear component is defined as:

$$\mathbf{V}^{(p)}_{\text{nonlin}} = \underbrace{\mathbf{V}_{\text{lin}} \left\lceil \otimes \right\rceil \mathbf{V}_{\text{lin}} \left\lceil \otimes \right\rceil \ldots \left\lceil \otimes \right\rceil \mathbf{V}_{\text{lin}}}_{p \text{ times}}, \tag{2}$$

where p indicates the degree of the polynomial, and the operation $\left\lceil \otimes \right\rceil$ produces all distinct monomials formed by pairwise multiplication of elements from the combined vectors. This allows the model to represent complex nonlinear couplings among the input variables.

The full feature vector for a single time step is then constructed by merging the linear representation, the nonlinear expansion, and a constant offset term:

$$\Psi_i = 1 \;\oplus\; \mathbf{V}_{\text{lin}} \;\oplus\; \mathbf{V}^{(p)}_{\text{nonlin}}. \tag{3}$$

The reconstruction of the desired signal X_i^{target} at time i is performed through a linear readout layer:

$$\mathbf{X}_i^{\text{rec}} = \mathbf{W}_{\text{out}}\, \Psi_i, \tag{4}$$

where $\mathbf{W}_{\text{out}}$ denotes the trainable output weight matrix.

We train and evaluate the NG-RC separately for each participant and for each reconstructed channel, so that every channel of every subject is assigned its own optimal set of hyperparameters (k, Δt, α, p). The available data consists of 60 epochs in total, which we split equally into a training set (30 epochs) and a held-out test set (30 epochs). The test set is used exclusively for the final performance comparison against other methods and is never involved in hyperparameter optimization.

Hyperparameter optimization is performed on the training set using a leave-one-out cross-validation scheme over the 30 training epochs. Specifically, for each candidate set of hyperparameters (k, Δt, α, p), we conduct 30 iterations. In each iteration, 29 epochs serve as the fitting subset and the remaining 1 epoch serves as the validation subset. Formally, for a given split s, let the fitting subset consist of epochs with indices $\mathcal{E}^{(s)}_{\text{fit}}$ and the validation epoch be $e^{(s)}_{\text{val}}$. For each epoch $e \in \mathcal{E}^{(s)}_{\text{fit}}$, we construct a feature matrix by stacking the augmented state vectors Ψ_i column-wise across all time steps within the epoch:

$$\mathbf{F}^{(e)} = [\Psi_{t_e^{(1)}} \mid \Psi_{t_e^{(2)}} \mid \ldots \mid \Psi_{t_e^{(T_e)}}] \;\in\; \mathbb{R}^{N_f \times T_e}, \tag{5}$$

where N_f is the feature dimension and T_e is the number of time steps in epoch e. The feature matrices from all fitting epochs are concatenated along the temporal axis:

$$\Psi_{\text{fit}}^{(s)} = [\mathbf{F}^{(e_1)} \mid \mathbf{F}^{(e_2)} \mid \dots \mid \mathbf{F}^{(e_{29})}] \in \mathbb{R}^{N_f \times T_{\text{fit}}^{(s)}}, \tag{6}$$

where $T_{\text{fit}}^{(s)} = \sum_{e \in \mathcal{E}_{\text{fit}}^{(s)}} T_e$. The corresponding target matrix $\mathbf{X}_{\text{fit}}^{\text{target}}$ is formed analogously. The output weights are then computed via ridge regression on the concatenated fitting data:

$$\mathbf{W}_{\text{out}}^{(s)} = \mathbf{X}_{\text{fit}}^{\text{target}} (\Psi_{\text{fit}}^{(s)})^{\text{T}} (\Psi_{\text{fit}}^{(s)} (\Psi_{\text{fit}}^{(s)})^{\text{T}} + \alpha \mathbf{I})^{-1}, \tag{7}$$

where α is the Tikhonov regularization coefficient and $\mathbf{I}$ is the identity matrix. The reconstruction quality is quantified using the coefficient of determination R^2 (8) which is evaluated on the held-out validation epoch $e_{\text{val}}^{(s)}$, and then averaged over all 30 leave-one-out iterations. The hyperparameters are optimized in the following ranges: $k \in [1, 2, \dots, 15]$, $\Delta t \in [\tau/4, \tau/2, \tau, 2\tau, 3\tau, 4\tau]$, $\alpha \in [10^{-3}, 10^{-2}, 10^{-1}, 10^{0}]$, and the polynomial degree $p \in \{1, 2\}$, where τ is the first minimum of the autocorrelation function of the target signal. The case $p = 1$ corresponds to a purely linear, delay-embedded feature vector, whereas $p = 2$ additionally includes the quadratic cross-terms defined in Eq. (2). The set (k, Δt, α, p) yielding the highest R^2 is selected as optimal.

After hyperparameter optimization, the final output weights are obtained by training on the entire training set (all 30 training epochs) using the optimal (k, Δt, α, p). The final model performance is then assessed on the held-out test set (30 epochs) and compared against alternative reconstruction methods.

2.3 Performance metric

Reconstruction quality is assessed using the coefficient of determination R^2. For an epoch with target signal $\mathbf{X}_e^{\text{target}} = [x_1, \dots, x_{T_e}]$ and reconstructed signal $\mathbf{X}_e^{\text{rec}} = [\hat{x}_1, \dots, \hat{x}_{T_e}]$, the R^2 score is given by:

$$R_e^2 = 1 - \frac{\sum_{t=1}^{T_e} (x_t - \hat{x}_t)^2}{\sum_{t=1}^{T_e} (x_t - \bar{x}_e)^2}, \tag{8}$$

where $\bar{x}_e$ is the epoch-wise mean of the target. An R^2 value of 1 indicates perfect reconstruction, 0 corresponds to the mean-predictor baseline, and negative values signify performance worse than this baseline.

To compare the reconstruction quality of NG-RC and spline interpolation from MNE-python we use the following metric of relative accuracy:

$$Q = \frac{R_{\text{NG-RC}}^2 - R_{\text{MNE}}^2}{1 - R_{\text{MNE}}^2} \times 100\%, \tag{9}$$

which determines how much of the gap between $R^2 = 1$ and R_{MNE}^2 is covered by NG-RC. When both methods produce the same accuracy, $Q = 0$. In case of MNE outperformance, $Q < 0$, otherwise it is > 0. Maximal value of $Q = 100\%$ can be achieved only if $R_{\text{NG-RC}}^2 = 1$.

3 Results

3.1 Reconstruction of noise-free EEG signals

We first evaluate the performance of NG-RC on artifact-free EEG data without additional noise contamination. For each of the 18 recording channels, the signal is reconstructed using the remaining 17 channels as input. The reconstruction quality is assessed separately in six frequency bands: δ (1–4 Hz), θ (4–8 Hz), α (8–13 Hz), β (13–30 Hz), γ (30–40 Hz), and the full 1–40 Hz range, and compared against the spherical spline interpolation method implemented in MNE-Python.

Figure 2 displays the spatial distribution of the relative accuracy metric Q (see Eq. 9) across the scalp. This metric quantifies the fraction of the performance gap between the MNE baseline and perfect reconstruction ($R^2 = 1$) that is recovered by NG-RC. Two main observations emerge from the topographic analysis. First, $Q > 0$ for all channels and all frequency bands, demonstrating that NG-RC consistently surpasses the spline interpolation method irrespective of brain region or oscillatory rhythm. Second, the spatial distribution of the improvement

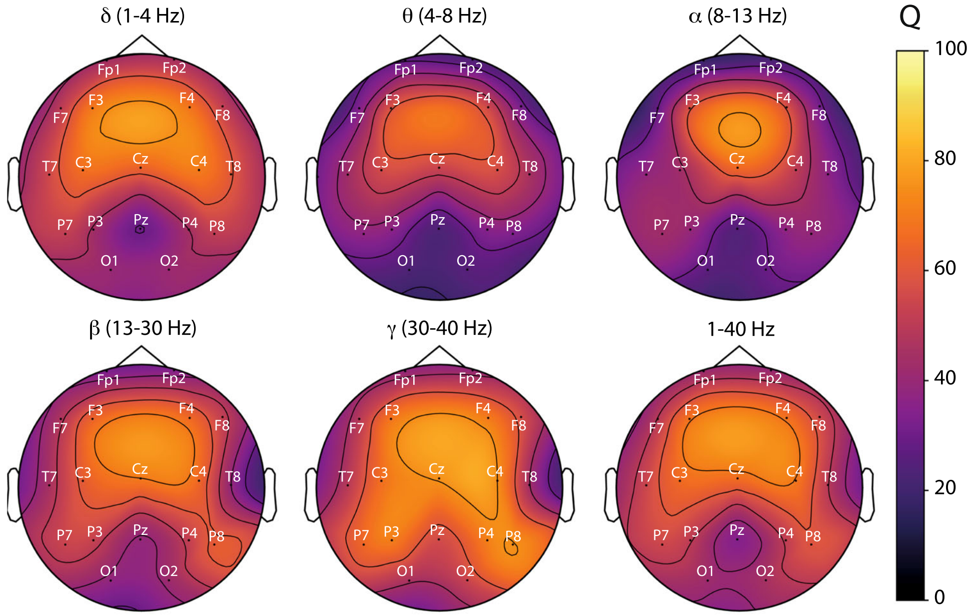

Fig. 2 The relative accuracy Q of the EEG-signals reconstruction using NG-RC with comparison to using spline interpolation of MNE-python package in different frequency bands: δ (1–4 Hz), θ (4–8 Hz), α (8–13 Hz), β (13–30 Hz), γ (30–40 Hz), and in all range of 1–40 Hz

is not uniform. In the frontal and central regions, particularly at electrodes F3, F4, and Cz, NG-RC exhibits a substantial advantage over MNE across the entire frequency spectrum. In the high-frequency β and γ bands, the superiority of NG-RC extends to virtually all scalp locations, whereas in the lower-frequency θ and α bands the performance gain is concentrated primarily in the frontal and central lobes.

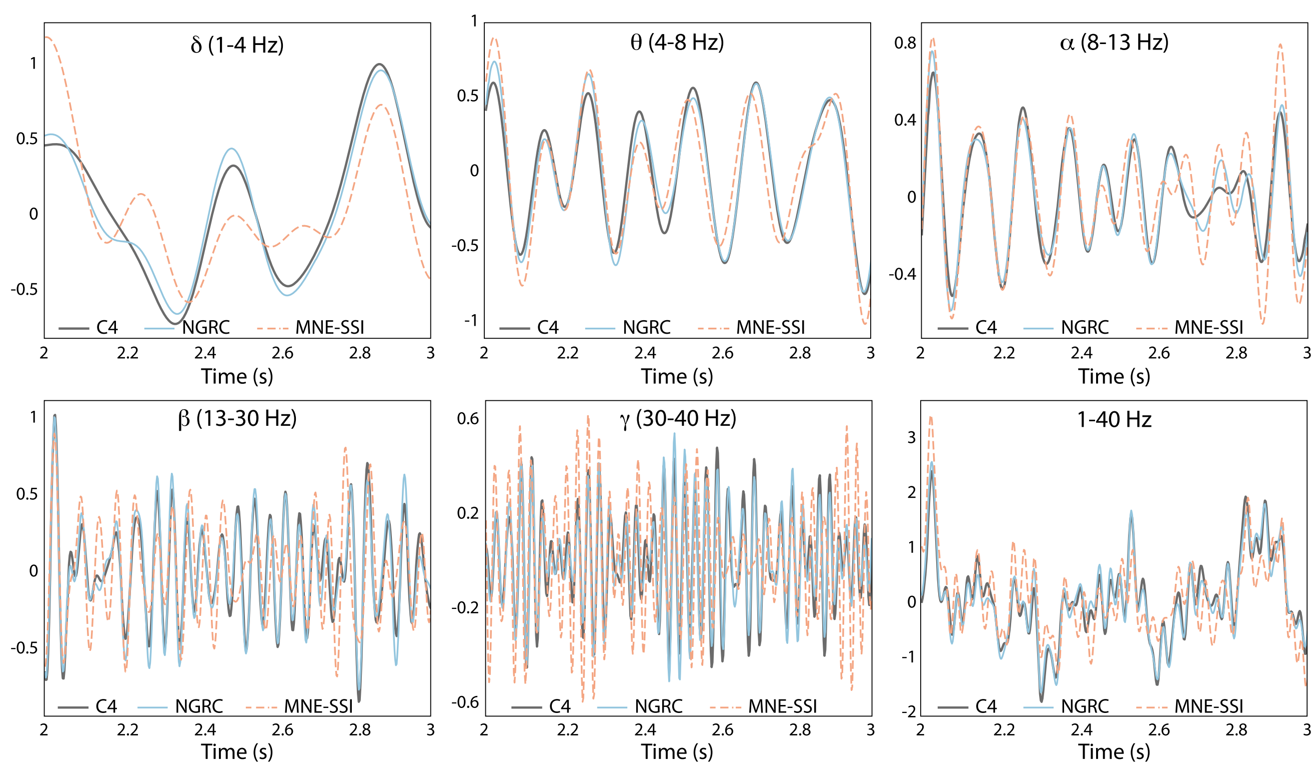

Fig. 3 Representative examples of C4-channel reconstruction using NG-RC (solid blue line) and MNE spline interpolation (dashed line) compared to the ground truth signal (solid green line) across six frequency bands: δ (1–4 Hz), θ (4–8 Hz), α (8–13 Hz), β (13–30 Hz), γ (30–40 Hz), and the full 1–40 Hz range

To provide a qualitative illustration of the reconstruction quality, Fig. 3 displays representative time series of the original and reconstructed signals for the C4 channel from a single participant. The signals are bandpass-filtered into the six frequency bands of interest and shown for a 1-second segment of a test epoch. The NG-RC reconstruction closely follows the ground truth across all bands, whereas the MNE spline interpolation exhibits visible deviations, particularly in the higher-frequency β and γ ranges where the rapid oscillations are poorly captured by purely spatial interpolation.

To provide a quantitative summary, Fig. 4 presents the median R^2 values for both methods and the corresponding relative-accuracy metric Q. For each subject and method, the median R^2 was first computed across all test epochs and the 18 EEG channels, and the corresponding subject-level Q value was then derived from these median R^2 values. The bars represent the median of the resulting subject-level values across the 24 subjects, and the error bars denote the corresponding between-subject standard deviation. The MNE baseline achieves its highest performance in the θ band ($R^2 = 0.734$) and maintains $R^2 > 0.6$ in the δ, θ, and α bands. However, its performance decreases sharply at higher frequencies, reaching $R^2 = 0.183$ in the β band and becoming negative in the γ band ($R^2 = -0.251$), indicating that, in the latter case, spline interpolation performs worse than the epoch-wise mean-predictor baseline. In contrast, NG-RC maintains $R^2 > 0.5$ across all six frequency ranges and achieves high reconstruction accuracy in the δ ($R^2 = 0.850$), θ ($R^2 = 0.849$), α ($R^2 = 0.789$), and full 1–40 Hz ($R^2 = 0.804$) ranges. Even in the challenging γ band, NG-RC attains $R^2 = 0.534$, which is comparable to the MNE performance in the α band. Consequently, Q is positive in all frequency bands, ranging from 38.6% in the α band to 64.5% in the γ band, where the spline-interpolation baseline is least effective and the relative improvement provided by NG-RC is therefore the largest.

Overall, these results indicate that NG-RC provides a systematic improvement over standard spline interpolation, with the advantage being most pronounced in high-frequency regimes where the linear, purely spatial interpolation fails to capture the finer oscillatory structure of EEG signals. The strong performance in frontal and central regions likely reflects the denser spatial sampling and richer inter-channel dependencies in these areas, which the temporal, delay-embedded feature construction of NG-RC is able to exploit effectively.

We also analyzed which hyperparameters the cross-validation selected. Across subjects and channels, the purely linear configuration ($p = 1$) was chosen far more often than the quadratic one ($p = 2$). This indicates that the reconstruction is governed by the linear, delay-embedded part of the feature vector, while the polynomial nonlinearity contributes little. At first sight this is surprising, because the nonlinear expansion is the distinctive feature of NG-RC. It is, however, consistent with the macroscopic nature of the scalp EEG signal. Each electrode does not record a single neuronal source but the spatially summed postsynaptic activity of large neuronal populations [29]. This summation acts as an averaging operation: the nonlinear fluctuations of the individual sources largely cancel, and the resulting macroscopic signal, together with its statistical relationships to the signals at other electrodes, becomes predominantly linear. A linear mapping between channels is therefore already close to optimal,

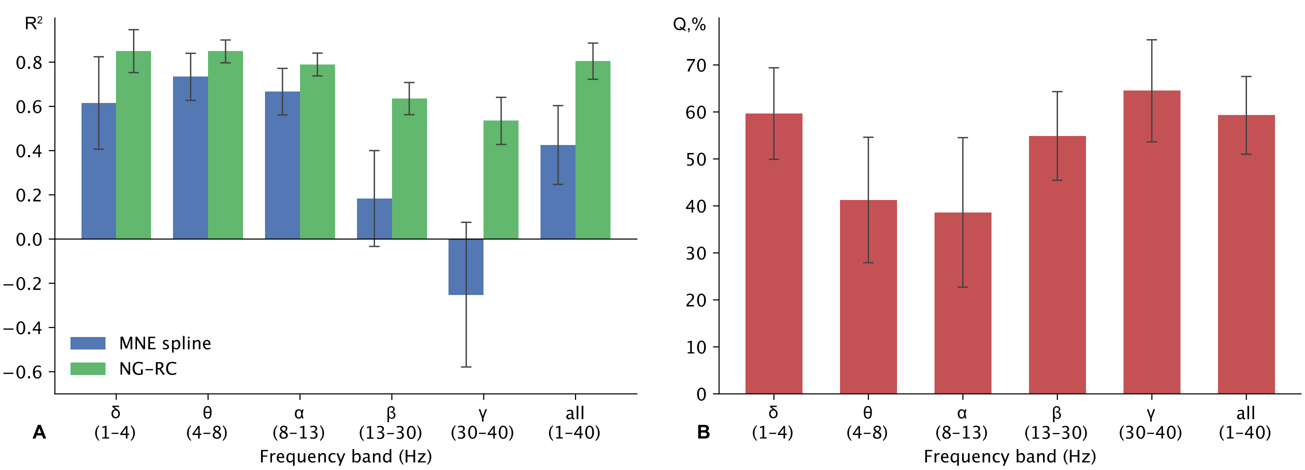

Fig. 4 Band-resolved reconstruction quality of NG-RC and spherical spline interpolation. **A** Coefficient of determination R^2 between the target and reconstructed signals for spline interpolation (MNE, blue) and NG-RC (green). **B** Relative accuracy Q (Eq. 9), defined as the fraction of the gap between the spline baseline and perfect reconstruction recovered by NG-RC. For each subject and method, the median R^2 was first computed across all test epochs and the 18 EEG channels. The corresponding subject-level Q values were then calculated from these median R^2 values. Bars represent the median of the resulting subject-level values across the 24 subjects, and whiskers denote their standard deviation across subjects. Results are shown for the five canonical EEG bands—δ (1–4 Hz), θ (4–8 Hz), α (8–13 Hz), β (13–30 Hz), and γ (30–40 Hz)—and the full 1–40 Hz range

and the quadratic terms have little to add. This interpretation is in line with recent evidence that macroscopic brain dynamics are, across a broad range of model classes, best described by linear models [30]. Accordingly, the advantage of NG-RC over spline interpolation does not arise from its nonlinearity but from its use of time-delayed inputs, which incorporate the temporal context of the signal that spline interpolation ignores entirely. This temporal information is most valuable in the β and γ bands, whose fast, low-amplitude oscillations are poorly described by the instantaneous, purely spatial model underlying spline interpolation.

3.2 Noise sensitivity analysis

To assess the robustness of the reconstruction methods against measurement noise, we conduct a controlled perturbation experiment. For each participant and each EEG channel independently, we generate a Gaussian noise signal $\xi(t) \sim \mathcal{N}(0, 1)$ with zero mean and unit variance. The noise is then scaled to a target intensity level and added to the original signal $X(t)$, producing a contaminated version:

$$\tilde{X}(t) = X(t) + \eta \cdot \sigma_X \cdot \xi(t), \tag{10}$$

where σ_X denotes the standard deviation of the clean signal $X(t)$ computed over the entire recording, and $\eta \in \{0.0, 0.1, 0.2, \ldots, 1.5\}$ is the noise intensity parameter controlling the relative perturbation amplitude. The noise realizations are generated independently for each channel and each participant, ensuring no false correlations are introduced across the electrode array.

The initial 1–40 Hz band-pass filtering described in Sect. 2.1 was performed once during preprocessing, before the introduction of noise. The additive Gaussian noise in Eq. (10) was added to the already band-limited signals in all training and test epochs, without subsequent 1–40 Hz re-filtering. For the band-resolved evaluation, both the noise-contaminated target signal and its reconstruction were subsequently filtered into the same canonical frequency bands before the calculation of R^2.

It has been previously shown [19, 31] that RC is effective in predicting the behavior of stochastic systems, so we can assume the stability of the reservoir operation under noisy data conditions.

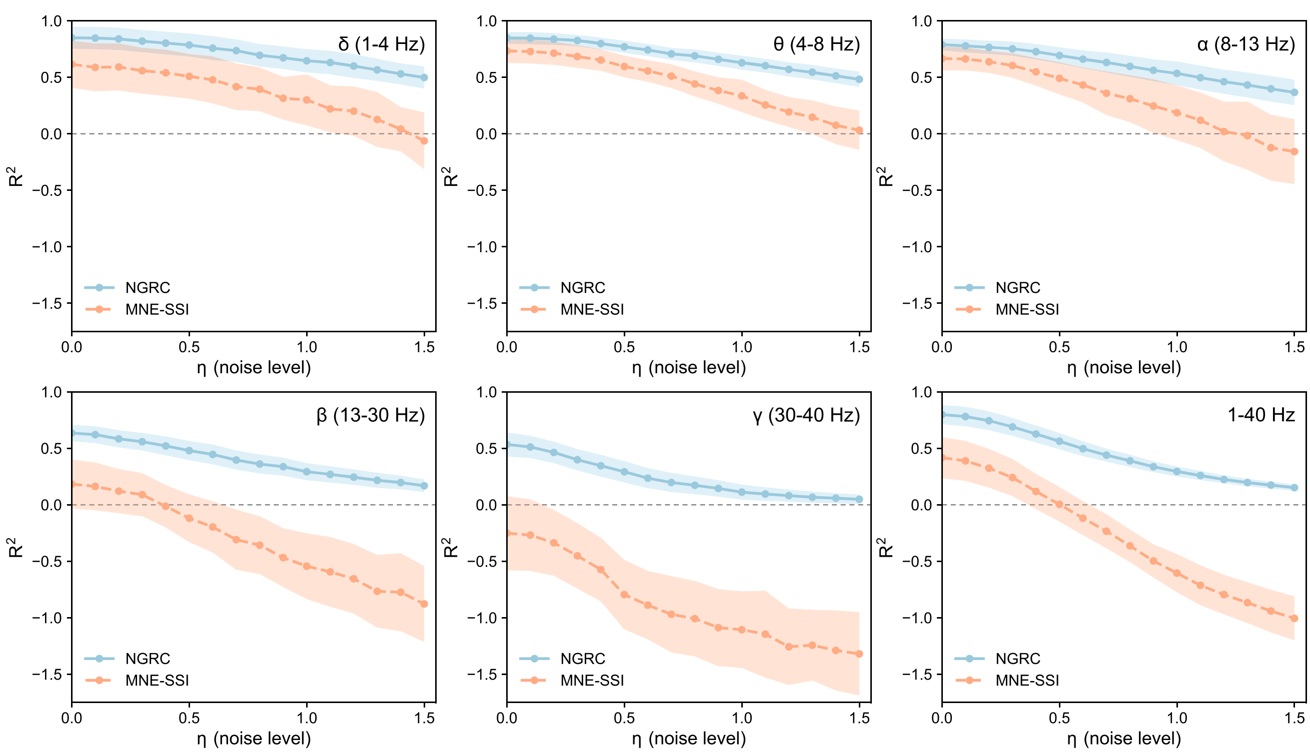

Fig. 5 The dependencies of reconstruction quality R^2 of NG-RC and baseline MNE methods on the noise level η in different frequency bands: δ (1–4 Hz), θ (4–8 Hz), α (8–13 Hz), β (13–30 Hz), γ (30–40 Hz), and in all range of 1–40 Hz. Solid and dashed lines represent the median R^2 computed over 30 test epochs, 18 EEG channels, and 24 subjects; shaded areas indicate ± 1 standard deviation across subjects

The noisy signals $\tilde{\mathbf{X}}_i = [\tilde{X}_{i1}, \tilde{X}_{i2}, \ldots, \tilde{X}_{iN_{\mathrm{in}}}]^{\mathrm{T}}$ serve as the input to the NG-RC model during both training and testing, while the target signal is also taken as the noise-contaminated version of the channel being reconstructed. This design mirrors a realistic scenario in which both the available measurements and the quantity to be estimated are subject to the same observational noise. The hyperparameters of the NG-RC model are kept fixed at the values optimized on clean data (see Sect. 2.2) to isolate the effect of noise on a given model configuration. For the baseline spline interpolation method, the same noisy signals are supplied as the input to the MNE-Python interpolation routine; one channel at a time is treated as missing and reconstructed from the remaining channels, exactly as in the noise-free case.

The reconstruction quality is evaluated on the held-out test set (30 epochs) using the coefficient of determination R^2 computed between the predicted signal and the noise-contaminated target. For each noise level η, frequency band, and method, we report the median R^2 across all 30 epochs, 18 EEG channels, and 24 subjects, with the translucent bands in Fig. 5 indicating the standard deviation across subjects.

Figure 5 presents the resulting noise sensitivity profiles. Across all frequency bands and all noise levels, the NG-RC model achieves higher median R^2 values than the MNE spline interpolation, and both methods degrade monotonically as the noise intensity η increases. The size of the gap between them, however, depends strongly on frequency. In the β (13–30 Hz), γ (30–40 Hz), and full-band (1–40 Hz) ranges the MNE method struggles considerably, with R^2 dropping toward zero or becoming negative at higher noise levels, while NG-RC retains substantially higher accuracy and continues to exploit inter-channel dependencies even for heavily corrupted signals. The lower-frequency δ (1–4 Hz), θ (4–8 Hz), and α (8–13 Hz) bands behave differently: both methods are far less sensitive to noise, their R^2 curves decline gradually, and the two approaches stay closer together. A possible explanation is that spline interpolation relies mainly on the spatial smoothness of scalp potentials. This assumption is more suitable for lower-frequency EEG components, whose scalp distributions are often broader and smoother. In contrast, β and γ activity changes more rapidly over time and is more sensitive to local spatial variations and high-frequency noise. These properties make purely spatial interpolation less effective, whereas NG-RC can benefit from the temporal context of the signal during reconstruction.

In summary, these findings indicate that the NG-RC-based reconstruction outperforms the conventional spline interpolation method across the full range of noise intensities, with the largest advantage in high-frequency regimes and under severe noise contamination, highlighting its potential for robust EEG signal recovery in real-world, noise-prone recording environments.

4 Conclusions

In this work, we have presented systematic investigation of Next-Generation Reservoir Computing for the reconstruction of multichannel EEG signals, including those contaminated by additive measurement noise. Using a dataset of 18-channel recordings from 24 participants, we benchmarked NG-RC against the widely used spherical spline interpolation method implemented in MNE-Python across six frequency bands and under controlled noise perturbations.

On clean EEG data, NG-RC consistently outperforms spline interpolation across all channels and all frequency bands. The improvement is most substantial in the β and γ bands, where the linear spatial interpolation largely fails (with R^2 dropping to 0.183 and -0.251, respectively), whereas NG-RC maintains R^2 values of 0.635 and 0.534. The relative accuracy metric Q reaches its maximum of 64.5% in the γ band, demonstrating that NG-RC recovers nearly two-thirds of the performance gap between the baseline method and perfect reconstruction. Topographically, the advantage of NG-RC is especially pronounced in frontal and central electrode sites, suggesting that the method effectively captures the richer inter-channel dependencies present in these densely sampled regions.

Under added noise, both methods degrade monotonically with increasing intensity, but NG-RC remains substantially more robust. The performance gap between the two methods widens as noise increases, particularly in high-frequency bands where the spline method becomes ineffective. In the lower-frequency δ, θ, and α bands, both approaches are relatively insensitive to moderate noise levels, reflecting the stronger spatial signature of high-amplitude slow oscillations. In contrast, the low-amplitude fast oscillations in the β and γ bands are poorly captured by purely spatial interpolation but are effectively recovered by NG-RC even under severe noise contamination, highlighting the critical role of temporal feature construction.

These results carry two practical advantages. Methodologically, NG-RC combines simplicity with strong performance: unlike deep learning approaches, it requires no iterative gradient-based training and has only a few transparent hyperparameters. In applied settings, its noise robustness makes it a candidate for real-world EEG monitoring, such as ambulatory recordings or mobile brain–computer interfaces, where electrode failures and environmental noise are common.

This study has several limitations. First, NG-RC is a data-driven method and, unlike spline interpolation, requires a training stage. In the present analysis, half of each recording was used for training, corresponding to 30 epochs. Although this is a relatively small training set, we did not systematically examine how much training data is needed for NG-RC to maintain its advantage. Second, the electrode layout was fixed and relatively sparse, with 18 channels. The magnitude of the difference between NG-RC and spline interpolation may depend on electrode density, because spline interpolation is expected to improve when neighboring electrodes are located closer to the target channel. Therefore, the performance of NG-RC under denser montages remains to be evaluated. Finally, the analysis was limited to a single experimental paradigm and 24 healthy participants, leaving open the question of how well the results generalize to other tasks, functional states, larger samples, and clinical populations.

As further research directions, it is of interest to identify the possibilities of restoring not only fast EEG signals, but also slow fMRI signals, which are increasingly considered as promising sources of information for the diagnosis of various brain diseases [32], including major depressive disorder [33], schizophrenia [34], disorder of consciousness [35], etc.

In conclusion, Next-Generation Reservoir Computing represents a data-driven alternative to conventional interpolation for EEG signal recovery. Its consistent superiority across frequency bands, particularly in challenging high-frequency and high-noise regimes, together with its conceptual simplicity and computational efficiency, make it suitable for EEG preprocessing in both research and clinical settings.

Acknowledgements The work was funded by the Russian Science Foundation (Grant No. 24-68-00030, https://rscf.ru/project/24-68-00030/).

Data availability statement The data that support the findings of this study are available from the corresponding author upon reasonable request.

References

1. E. Niedermeyer, F.L. Silva. *Electroencephalography: Basic Principles, Clinical Applications, and Related Fields*, 5th edn (Lippincott Williams & Wilkins, 2005)
2. N.S. Frolov, V.S. Khorev, V.V. Grubov, A.A. Badarin, S.A. Kurkin, V.A. Maksimenko, A.E. Hramov, A.N. Pisarchik, Stabilization of an unstable equilibrium of a balance platform due to short-term training. Chaos Solitons Fractals **158**, 112099 (2022)
3. C.P. Lisgaras, L.M. Prida, E. Bertram, M. Cunningham, D. Henshall, A.A. Liu, V. Gnatkovsky, S. Balestrini, M. Curtis, A.S. Galanopoulou et al., The role of electroencephalography in epilepsy research—from seizures to interictal activity and comorbidities. Epilepsia **66**(5), 1374–1393 (2025)
4. V.V. Grubov, S.I. Nazarikov, S.A. Kurkin, N.P. Utyashev, D.A. Andrikov, O.E. Karpov, A.E. Hramov, Two-stage approach with combination of outlier detection method and deep learning enhances automatic epileptic seizure detection. IEEE Access **12**, 122168–122182 (2024)
5. A. Poblano, R. Santana-Miranda, Utility of electroencephalography in the evaluation of sleep disorders. Revista médica del Hospital General de México **88**(3), 146–154 (2025)
6. E. Sitnikova, A.E. Hramov, V. Grubov, A.A. Koronovsky, Rhythmic activity in EEG and sleep in rats with absence epilepsy. Brain Res. Bull. **120**, 106–116 (2016)
7. J. Lanzone, F. Motolese, L. Ricci, F. Tecchio, M. Tombini, F. Zappasodi, A. Cruciani, F. Capone, V. Di Lazzaro, G. Assenza, Quantitative measures of the resting EEG in stroke: a systematic review on clinical correlation and prognostic value. Neurol. Sci. **44**(12), 4247–4261 (2023)
8. B. Dalla Bernardina, G. Cantalupo, C.A. Tassinari, The role of the EEG in the diagnosis of epileptic encephalopathies, in *EEG: The First 100 Years: Past, Present and Future of Electroencephalography* (Springer, 2025), pp. 141–152
9. M. Verboom, R. Berg, M. Ruit, M. Jagt, Prognostic value of electroencephalography in critically ill adult patients with traumatic brain injury: a systematic review. J. Neurotrauma **43**(1–2), 13–34 (2026)
10. V.V. Grubov, A.K. Kuc, S.A. Kurkin, D.A. Andrikov, N. Utyashev, V.A. Maksimenko, O.E. Karpov, A.E. Hramov, Harnessing long-range temporal correlations for advanced epilepsy classification. PRX Life **3**(1), 013005 (2025)
11. N. Frolov, E. Pitsik, V. Grubov, A. Badarin, V. Maksimenko, A. Zakharov, S. Kurkin, A. Hramov, Perceptual integration compensates for attention deficit in elderly during repetitive auditory-based sensorimotor task. Sensors **23**(14), 6420 (2023)
12. A. Biasiucci, B. Franceschiello, M.M. Murray, Electroencephalography. Curr. Biol. **29**(3), 80–85 (2019)
13. O. Drapkina, A. Savosenkov, S. Gordleeva, S. Kurkin, A. Badarin, N. Grigorev, A. Udoratina, A. Kiselev, V. Kazantsev, A. Hramov, Characteristics of the specific brain functional network correlate with the latency of motor imagery. Eur. Phys. J. Spec. Top. **233**(3), 479–488 (2024)
14. A.E. Hramov, V.A. Maksimenko, A.N. Pisarchik, Physical principles of brain–computer interfaces and their applications for rehabilitation, robotics and control of human brain states. Phys. Rep. **918**, 1–133 (2021)
15. J.A. Urigüen, B. Garcia-Zapirain, EEG artifact removal—state-of-the-art and guidelines. J. Neural Eng. **12**(3), 031001 (2015)
16. A. Gramfort, M. Luessi, E. Larson, D.A. Engemann, D. Strohmeier, C. Brodbeck, R. Goj, M. Jas, T. Brooks, L. Parkkonen, M. Hämäläinen, MEG and EEG data analysis with MNE-Python. Front. Neurosci. **7**, 267 (2013)

17. F. Perrin, J. Pernier, O. Bertrand, J.F. Echallier, Spherical splines for scalp potential and current density mapping. Electroencephalogr. Clin. Neurophysiol. **72**(2), 184–187 (1989)
18. M. Lukoševičius, H. Jaeger, Reservoir computing approaches to recurrent neural network training. Comput. Sci. Rev. **3**(3), 127–149 (2009)
19. A.E. Hramov, N. Kulagin, A.N. Pisarchik, A.V. Andreev, Strong and weak prediction of stochastic dynamics using reservoir computing. Chaos Interdiscip. J. Nonlinear Sci **35**(3), 033140 (2025)
20. A. Badarin, A. Andreev, V. Klinshov, V. Antipov, A.E. Hramov, Hidden data recovery using reservoir computing: adaptive network model and experimental brain signals. Chaos Interdiscip. J. Nonlinear Sci. **34**(10), 103121 (2024)
21. A.V. Andreev, A.N. Pisarchik, N. Kulagin, R. Jaimes-Reátegui, G. Huerta-Cuellar, A.A. Badarin, A.E. Hramov, Stochastic cloning of dynamical systems with hidden variables. Phys. Rev. E **112**(1), 015303 (2025)
22. A. Badarin, V. Klinshov, P. Smelov, A. Andreev, Reservoir computing reconstructs blood-oxygen-level-dependent signals: whole-brain modeling study. Eur. Phys. J. Spec. Top. **234**(15), 4497–4504 (2025)
23. N. Kulagin, A. Andreev, A.A. Koronovskii, O.I. Moskalenko, A.P. Sergeev, A. Badarin, A.E. Hramov, Intermittency in predicting the behavior of stochastic systems using reservoir computing. Phys. Rev. E **111**(2), 024209 (2025)
24. H. Jaeger, H. Haas, Harnessing nonlinearity: predicting chaotic systems and saving energy in wireless communication. Science **304**(5667), 78–80 (2004)
25. D.J. Gauthier, E. Bollt, A. Griffith, W.A. Barbosa, Next generation reservoir computing. Nat. Commun. **12**(1), 5564 (2021)
26. W.A. Barbosa, A. Griffith, D.J. Gauthier, Learning spatiotemporal chaos using next-generation reservoir computing. Chaos: Interdiscip. J. Nonlinear Sci. **32**(9), 093137 (2022)
27. J.A. Platt, S.G. Penny, T.A. Smith, T.-C. Chen, H.D. Abarbanel, Robust forecasting using predictive generalized synchronization in reservoir computing. Chaos: Interdiscip. J. Nonlinear Sci. **31**(12), 123118 (2022)
28. A.A. Badarin, V.M. Antipov, O.M. Drapkina, A.R. Kiselev, Spatiotemporal dynamics of functional connectivity networks in EEG-based motor imagery. Russ. Open Med. J. **14**(4), 423 (2025)
29. G. Buzsáki, C.A. Anastassiou, C. Koch, The origin of extracellular fields and currents—EEG, ECoG, LFP and spikes. Nat. Rev. Neurosci. **13**(6), 407–420 (2012)
30. E. Nozari, M.A. Bertolero, J. Stiso, L. Caciagli, E.J. Cornblath, X. He, A.S. Mahadevan, G.J. Pappas, D.S. Bassett, Macroscopic resting-state brain dynamics are best described by linear models. Nat. Biomed. Eng. **8**(1), 68–84 (2024)
31. A.E. Hramov, N. Kulagin, A.V. Andreev, A.N. Pisarchik, Forecasting coherence resonance in a stochastic Fitzhugh–Nagumo neuron model using reservoir computing. Chaos Solitons Fractals **178**, 114354 (2024)
32. S.A. Kurkin, A.N. Pisarchik, L.A. Mayorova, A.E. Hramov, Evolution of methods for assessing fMRI-based functional networks: from classical pairwise connectivity to higher-order interactions. Phys. Rep. **1174**, 1–66 (2026)
33. D. Stoyanov, V. Khorev, R. Paunova, S. Kandilarova, D. Simeonova, A. Badarin, A. Hramov, S. Kurkin, Resting-state functional connectivity impairment in patients with major depressive episode. Int. J. Environ. Res. Public Health **19**(21), 14045 (2022)
34. M. Giraldo-Chica, N.D. Woodward, Review of thalamocortical resting-state fMRI studies in schizophrenia. Schizophr. Res. **180**, 58–63 (2017)
35. S. Kurkin, L. Mayorova, V. Khorev, E. Pitsik, M. Radutnaya, E. Bondar, A. Hramov, Multiscale fMRI analysis reveals hierarchical network disruptions underlying disorders of consciousness. Chaos Solitons Fractals **200**, 117008 (2025)